# Distributed Sensing for Soft Worm Robot Reduces Slip for Locomotion in Confined Environments

Akhil Kandhari[1], Matthew C. Stover[1], Prithvi R. Jayachandran[1], Alexander Rollins[2], Hillel J. Chiel[3], Roger D. Quinn[1], and Kathryn A. Daltorio[1]

[1]Department of Mechanical and Aerospace Engineering,
Case Western Reserve University, Cleveland, OH 44106, USA
[2]Mayfield High School, Cleveland, OH 44106, USA
[3]Departments of Biology, Neurosciences, and Biomedical Engineering,
Case Western Reserve University, Cleveland, OH 44106, USA
{axk751,kam37}@case.edu

**Abstract.** Earthworms are soft-bodied animals with mechanosensory organs that allow them to bend and contort, and adapt to external perturbations. To mimic these attributes of the earthworm on a robotic platform, we designed and constructed a new robot: Distributed-Sensing Compliant Worm (DiSCo-Worm) Robot. DiSCo-Worm is equipped with 36 Force Sensing Resistors (6 per segment) that allow the robot to detect external constraints and 12 flexible stretch sensors (2 per segment) that allow for tracking the shape of the robot. We show the ability of the robot to navigate in constrained spaces using an open-loop, time-based controller and a closed-loop sensory feedback controller. The results indicate that the robot can sense external constraints and its internal state (longitudinal extension of each segment) and use this information to change its state of either expanding in diameter, contracting in diameter or anchoring. Sensory feedback reduces high forces that otherwise result in damage to the robot by stopping actuation shortly after contact. In this way, each segment applies forces 33% to 80% (based on the location of the sensor) of its weight, when locomoting between two parallel surfaces. Using a closed-loop controller, the robot is able to adapt to its environment and almost eliminates forward slip, which accounts for 58% of the total motion in case of open-loop control.

**Keywords:** Sensors, Earthworm-like robots, Soft-robotics.

## 1    Introduction

Compliant or "soft" robots that can undergo large deformations are promising because of their ability to passively adapt their shape to the environment (for example in grasping an arbitrary object [1]), store collision energy (for example in running legs [2]), and recover from damage (for example bouncing back into shape after being compressed [3]). There are many instances where performance is improved by compliance, but often the cost of compliance is uncertainty.

As sensor technology improves, it is possible to put tactile sensors in new places and with softer materials. However, the value of such sensors for soft-body locomotion is not yet established.

To assess the added value of such sensors, we have built a new worm-like robot with a total of 49 sensors and 12 actuators. Unlike our previous Compliant Modular Mesh Worm Robot which relied only on smart servomotors to control the diameter of each segment and infer ground contact [4], here each segment diameter is controlled independently on the left and right side, contact pressures are measured directly with force-resistive sensors, and stretch sensors assess body shape.

While there have been many other worm-like robots [3, 5-10], contact sensing has not been explored in most cases. Thus, this platform is valuable for (1) implementing closed-loop control for constrained environments, (2) better understanding mechanics of peristaltic locomotion in animals and robots, (3) determining critical requirements for sensor operation and placement, and (4) in future work, validating simulations [11] of modular soft bodies.

In this article we discover that (a) the forward progress under open loop control is largely due to slip, (b) the actuators work harder and longer in open loop, wasting energy and risking damage to structure and actuation cables, and (c) the movements of the closed loop robot incur less slip, which is a key cause of imprecision.

## 2 Background

Soft-bodied invertebrates such as earthworms can access constrained environments by contorting their bodies in order to comply with their surroundings. The multi-segmented body of an earthworm incorporates circumferential and longitudinal muscles. Due to hydrostatic coupling, activation of a segment's circumferential muscles causes it to contract in diameter while extending in length, whereas activation of longitudinal muscles causes the segment to shorten in length and expand in diameter [12]. Peristaltic waves of segment contractions and expansions along the length of the earthworm's body [13] cause the soft-bodied animal to locomote. This coupling between the length and diameter of a segment [12] allows the longer contracted segments to lift off the ground while the circumferentially expanded segments rest on the ground to anchor forward locomotion [14]. While complying with their surroundings, earthworms are also capable of exerting forces radially and laterally against their environment to break up compacted soil, create and enlarge burrows, and resist extraction from their burrows by predators.

During peristaltic locomotion, sensory feedback allows the animal to adapt to environmental perturbations [15]. Sensory feedback from various mechanosensory organs and stretch, touch, and pressure receptors [16] allow the animal to maintain rhythmic peristaltic locomotion by modulating motor patterns [13]. Setae, present on the body of the earthworm, serve as mechanoreceptors that allow it to adapt to its environment and crawl smoothly even on rough surfaces [15].

Soft-bodied robots have been shown to be mobile in constrained-space applications [5,10,17-20]. In simulation, we have shown that a worm-like robot can be more efficient in crawling through constrained environments with contact sensing [21]. Specifically, we have shown that a worm-like robot crawling through a narrowing in a pipe will exert more energy because the segments lose energy to friction and slip. However, if ground contact forces can be sensed, the Cost of Transport (COT) can be reduced. This paper is the first step in implementing such a controller on a physical robot.

## 3      Robot design

Our Distributed-Sensing Compliant Worm robot (DiSCo-Worm) (Figure 1) has a modularly assembled soft mesh body, like our previous robot CMMWorm [6]. The mesh of the robot consists of short "links" of flexible tubing connected via 3-D printed "vertex pieces", that allow relative rotation. Links of tubes and vertex pieces are assembled to form a rhombus, such that rotation of the vertex pieces will cause the aspect ratio of a rhombus to change. These rhombuses are connected in a ring-like structure to form a segment.

Each of the six modular segments has two actuators, one for each half of the segment [22]. Connected to each actuator spool, a cable travels halfway around the circumference of the segment, either controlling the left or the right half of the segment. The actuators spool in the cable causing the segment to contract in diameter, while extending in length, equivalent to the circumferential muscles in earthworms. The diameter of the segment is constrained by the amount of cable spooled in. Longitudinal springs placed along the length of each segment perform similarly to the longitudinal muscle of an earthworm's body. On removal of the circumferential actuation force that causes the robot to decrease in diameter, these longitudinal springs return the segment to the maximum diameter as the circumferential cable is spooled out. Sequential actuation of the segments causes a wave of circumferential contractions and expansions to travel down the length of the body. This results in peristaltic locomotion opposite to the direction of the wave's travel.
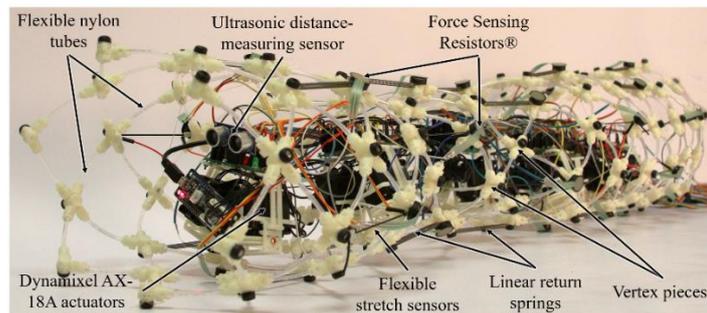


**Fig. 1.** Distributed-Sensing Compliant Worm robot (DiSCo-Worm) during a peristaltic wave on flat surface. The various components of the robot mesh including the sensors and actuators are labelled.

Unlike other worm robots, DiSCo-Worm incorporates a suite of pressure and stretch sensors along the surface of its body. This network of distributed sensors allows the robot to sense external perturbations and constraints, while keeping track of its own configuration. Each sensor works independently. Each segment incorporates six Force Sensing Resistors® (FSR-402) and two flexible stretch sensors. The FSR-402 sensors are placed on each vertex piece around the circumference of each segment (Figure 2), in order to detect external loads that may act on the robot radially (for example, from the inner surface of a pipe). FSR sensors exhibit a decrease in resistance with increase in force applied to the 14.7mm active area of the sensor. This decrease in resistance corresponds to external loads the robot experiences.

Because the readings from the FSR sensors are independent of segment position, we also added conductive stretch sensors that run along the length of the segments (one on each side). As the segment extends in length, the resistance of the stretch sensors increases, directly correlated to the extended length of the segment. Because the radius of a segment is kinematically constrained to decrease with length, these sensors indicate the shape of the segment.
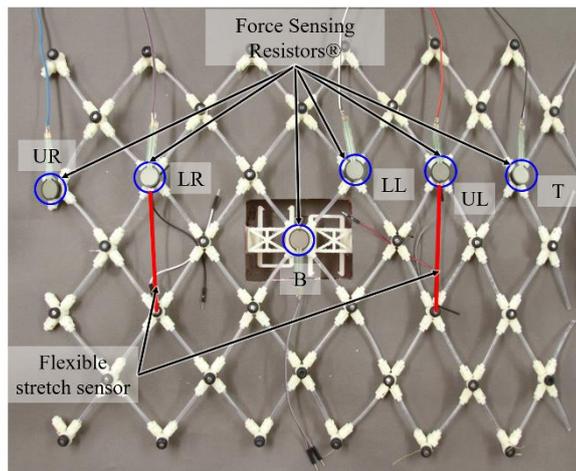


**Fig. 2.** Sensor configuration of a single segment placed flat on a surface. The FSR sensors are marked by circles around them. Stretch sensors are highlighted in red. UR: Upper Right, LR: Lower Right, UL: Upper Left, LL: Lower Left, T: Top, B: Bottom. Left and right vertex pieces join to form the ring-like structure and anterior and posterior segments are connected to the vertex pieces at the top and bottom of the figure.

To detect objects in the robot's path, the first segment is specialized with the addition of an HC-SR04 ultrasonic distance-measuring sensor. This allows the robot to respond to obstacles in the robot's path.

DiSCo-Worm thus has distributed sensing: Each of the six segments has eight sensors and the first segment has an ultrasonic sensor, for a total of forty-nine sensors to determine its configuration and environment.

# 4 Electronics and control

DiSCo-Worm is actuated by twelve Dynamixel AX-18A actuators connected to an ArbotiX-M microcontroller. The actuators are powered using an off-board DC power supply at a constant voltage of 11.8V. All forty-nine sensors are wired back to an off-board Mayhew Labs MUX Shield II connected to the ArbotiX-M microcontroller. The MUX Shield II allows the ArbotiX-M microcontroller to extend its total number of analog ports from 8 to 53.

A 3×1 waveform, where 3 represents the number of segments per wave (including inactive suspended segments) and 1 represents the number of waves along the body, was used for all tests throughout this paper. The 3×1 wave consists of an expanding segment, a contracting segment and an inactive suspended (contracted) segment between the two active segments. The active actuators are commanded to move at a specified speed with maximum torque. All other inactive segments during a wave are expanded to their maximum allowable diameter, for anchoring. An open-loop time-based control is compared to a closed-loop control scheme where both controllers always maintain this pattern.

With open-loop (time-based) control, actuators are configured to move for a fixed duration. This duration is based on the time it takes for a segment to contract to its minimum possible diameter of 13 cm from its maximum (initial) diameter of 22 cm at a constant actuator speed. The next set of actuators in the wave sequence are activated immediately after the previous duration terminates.

With closed-loop control, speeds are the same but the duration is limited by the forces measured at the FSRs (during radial expansion) and the extension measured with the conductive stretch sensors (during radial contraction). The microcontroller interprets the data from the sensors to control the actuators such that an expanding segment is commanded to move until a preset force threshold value is reached. The preset was established via single-segment testing to achieve a desired normal force. A contracting segment is commanded to move until a preset stretch sensor threshold value is reached, correlating to its maximum allowable extension. In this control scheme, the two segments are actuated independently. If a contracting or expanding segment reaches its threshold value first, the segment stops and waits for its corresponding active segment to stop. The next set of actuators are activated once both segments in the previous wave sequence stop. In case an external threshold is not reached (no external constraint), a time-based threshold is set in order to stop the expanding segment once it reaches its maximum diameter.

# 5 Experimental Methods and Results

## 5.1 Single Segment in Pipe

To demonstrate contact forces in a radially symmetric environment, a single segment of DiSCo-Worm was tested inside a pipe with inner diameter of 20.32 cm (92% of the nominal maximum diameter). The segment was first contracted and inserted in a pipe

and then cycled between successive expansions and contractions. This allowed us to calibrate the force applied by FSR sensors on an external constraint. A video from the lateral view allowed us to map the stretch sensor data to segment length. Tracker (version 4.10) video analysis software was used to measure the length of the segment.
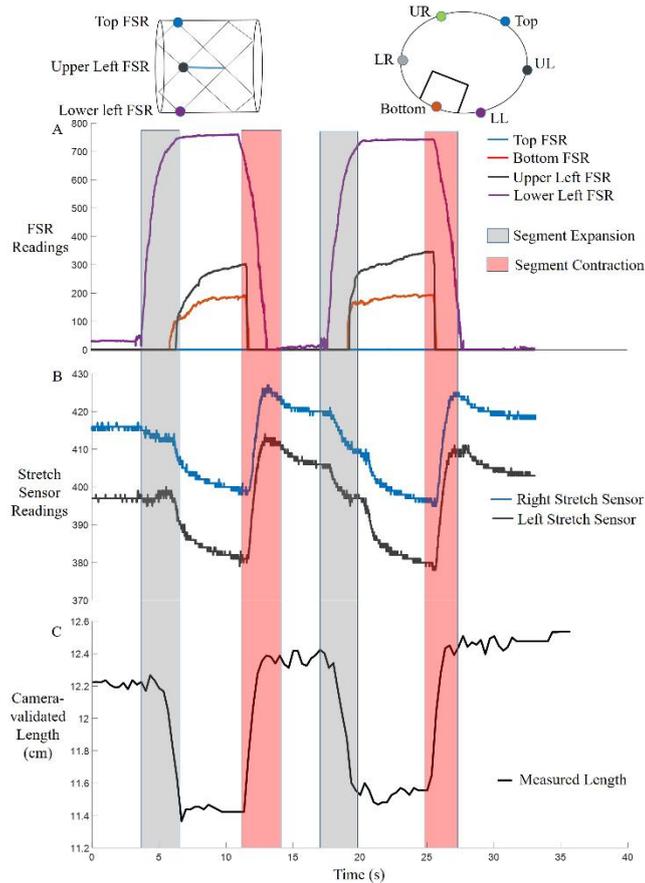


**Fig. 3.** Expansion of a single segment within a pipe of 20.32 cm inner diameter (orientation of the segment when placed within the pipe is shown on top). (A) FSR readings from four pressure sensors along the circumference of the segment indicate the segment encountering the inner wall of the pipe. The segment diagram on top shows the placement of the sensors around the circumference when viewed from a transverse view. Lower Left sensor shows large force readings on the onset of segment expansion. On completion of expansion, the three FSR readings (Bottom, Upper Left and Lower Left) indicate continuous contact with the inner wall of the pipe until contraction starts at which point no radial force is applied on these sensors. (B) Stretch sensor measurement from both right and left side of the segment shows an increase in resistance as the segment begins to extend in length. The offset between the two stretch sensors is due to the initial lengths of the sensors being different. During operation, we subtract the current reading from the reading obtained at maximum possible extension. (C) Measured side length of the segment using video analysis indicating the expansion and contraction cycle aligned with sensory data.

The placement of each FSR relative to gravity determines the order in which contact forces are sensed during radial expansion (Figure 3). Consider the 4 sensors on the left side of the body: in this case, the Lower Left (LL) FSR was at the bottom of the pipe, so it measures contact forces first. Then the Upper Left FSR, and Bottom FSR also made contact. The positioning of the segment is such that these two sensors are placed on vertex pieces opposite each other. However, due to the weight of the segment, UL FSR experiences a larger force compared to the Bottom FSR. The Top (T) FSR sensor never records any force, as it never encountered the inner wall of the pipe because gravity keeps the soft structure in a non-circular, deformed shape. The LL FSR sensor experiences a total force of 2.9 N which is the entire weight of a segment, whereas UL and bottom FSR sensors experience 0.5 N.

Stretch sensors are more accurate during radial contraction than during extension, which suits our need to limit contraction. During radial contraction, as the segment length increases, the values recorded from these sensors also increase. Since the segment uniformly contracts and expands, both these sensors exhibit a similar trend. However, on segment expansion, the values do not directly correlate to segment length. This is because the sensors have a few resistive artifacts (i.e., hysteresis). When stretched into position and released, the resistance slightly increases upon release, and decays exponentially to its resting resistive values. Figure 3 shows that the stretch sensor values start to decay during the suspension phase while the length of the segment is still constant.

## 5.2    Locomotion between Parallel Substrates

DiSCo-Worm with all six segments and 49 sensors locomoted between two parallel wooden surfaces set 16 cm apart (72% of initial maximum diameter (Figure 4)), using both open-loop and closed-loop control schemes. Results from these tests are summarized in this section.

During closed loop control, the sensors stop expansion after contact (Figure 5A). Note that between two parallel constraints, the figure shows that only the top and bottom sensors contact the ground. The threshold set (dashed lines, Figure 5A) indicate when the top or bottom have sufficient normal force to stop further expansion and allow anchoring of the segment. The bottom FSR sensor placed directly underneath the actuator mount experiences a high normal force, due to the weight of the segment resting on it. During expansion, on coming in contact with the constraint, the normal force on the Top FSR sensor increases the set threshold, thereby stopping any further expansion of the segment. It can be observed that during contraction and the suspended phase of the wave, the sensor reading for the bottom sensor indicates no contact with the ground. In contrast, during the anchoring phase of the peristaltic cycle, the bottom sensor measures large values, indicating the anchoring phase.

The bottom FSR sensor exerts a force of 2.3 N (80% of segment weight); compliance between adjacent segments prevents the segment from exerting 100% of its weight on the surface. The top FSR sensor experiences a maximum force of 1.0 N which quickly decreases due to motion of the other segments.
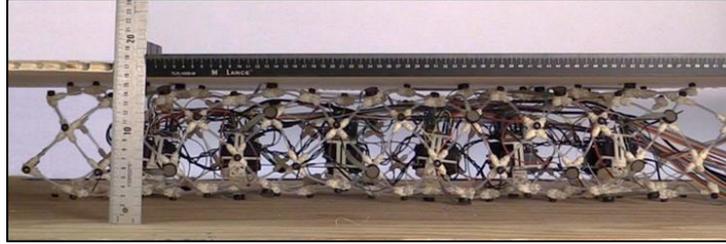
**Fig. 4.** DiSCO-Worm locomoting through two parallel horizontal wooden surfaces. The distance between the two surfaces was set at 16 cm. Both the open-loop controller and closed-loop controller were tested in the same constrained environment.

Stretch receptors indicate increase in resistive values when the segment undergoes contraction (Figure 5B). The threshold for the stretch sensors indicates when the segment reaches maximum longitudinal extension with some allowance. On reaching this preset threshold, the contraction phase of the actuation is stopped. During the expansion phase, the resistive values of the stretch sensors decay to their initial values, similar to the case of a single segment.

Actuator positions logged using the actuators encoder allow for tracking all four phases of the 3×1 peristaltic cycle (expansion, anchoring, contraction, suspension) and aligning with sensory feedback information.

How does limiting the duration of each step affect behavior? In 50 seconds, the closed loop control resulted in 5.04 cm progress over 7 peristaltic waves, whereas the open loop controller resulted in 10.43 cm over 5 peristaltic waves. Thus, as a result of the feedback control, the robot takes smaller steps adapting to its environment with an overall speed of 48% of the open loop speed. Although the open-loop movements are faster, they are less precise, as we describe below.

During open-loop control, there is a large amount of slip in both forward and backward directions. Slip occurs when segments move during anchoring phases. Slip is measured at the contact point using video analysis. For the open-loop controller, the segment slipped backward by 8.67 cm. If no backward slip had occurred, the total forward progress of the segment using an open-loop controller would have been 19.1cm. Using the closed-loop controller, the robot experienced backward slip of 6.70 cm, so there is less backward slip. Most of the backward slip, in both cases, was experienced during the contraction and suspension phase of the peristaltic cycle. Although both control schemes have high backward slip, forward slip in the case of open-loop control is higher than that of closed-loop control. With open-loop control, the robot progressed by approximately 6.10 cm during its anchoring phase. In contrast, the closed-loop controller did not progress noticeably during its anchoring phase. The maximum longitudinal extension in both cases was similar, but due to forward slip, segments in open-loop control contribute to larger progress. For some applications, slip in any direction is undesirable as it leads to imprecise control. Out of the total progress made by the open-loop controller, 58% was due to slip in the forward direction (at a time that the segment should have been anchoring). During slip, the upper and bottom surface of the

segment was in continuous contact with the external constraint. If there was no forward slip, the robot would have progressed by 4.3 cm for the open-loop controller.
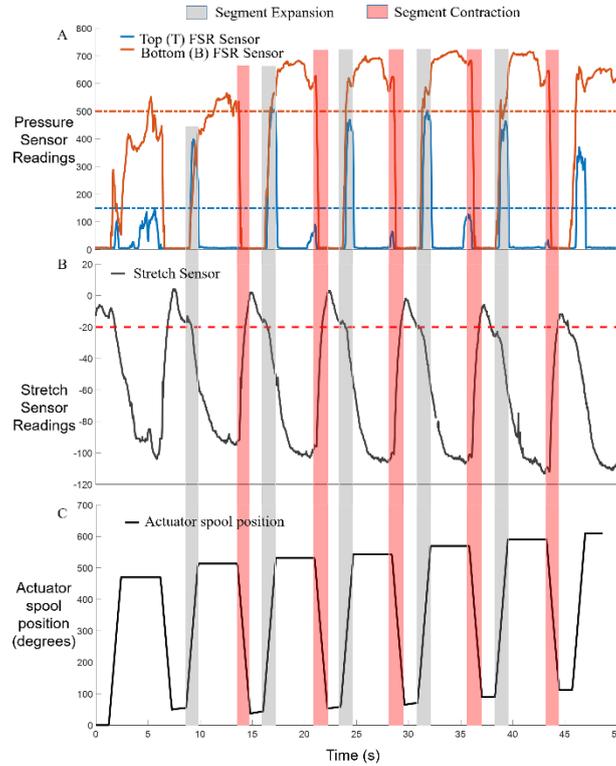


**Fig. 5.** Data recorded from the 2nd segment using the closed-loop controller as the robot was allowed to locomote between two parallel horizontal surfaces. (A) Sensory information from the Top and Bottom FSR indicating when the robot came in contact with the external constraint. The robot rests on ground so the bottom FSR reading is high when the segment is anchoring. The segment then contracts until it is completely lifted away from the ground (all FSR for that segment read zero). Then the segment expands causing the bottom and also the top FSR sensors to make contact with the substrates (both top and bottom FSR show contact forces). Due to the compliance of the structure, as the adjacent segments move, the top sensor loses contact, thus exhibiting no contact during the anchoring phase. The dashed orange and blue line indicates the preset force threshold for the closed-loop controller for the Bottom and Top FSR respectively. (B) Data from stretch sensor indicates longitudinal extension of the segment during contraction phase. Stretch sensor's resistance increases with an increase in length. The maximum extension that the stretch sensor experiences is set to zero. At zero, the contracting segment is at its minimum possible diameter. Negative values indicate the length of the stretch sensor is shorter than its maximum extension. Zero indicates that the segment has reached its maximum extension and any further extension can cause the robot to break. By setting the maximum extension, we eliminate any pre-existing discrepancies between stretch sensors (the offset observed between the left and right side in Figure 3). (C) Actuator position logged aligned with sensor data showing the four different phases of the peristaltic 3×1. The expansion and contraction phase are highlighted.
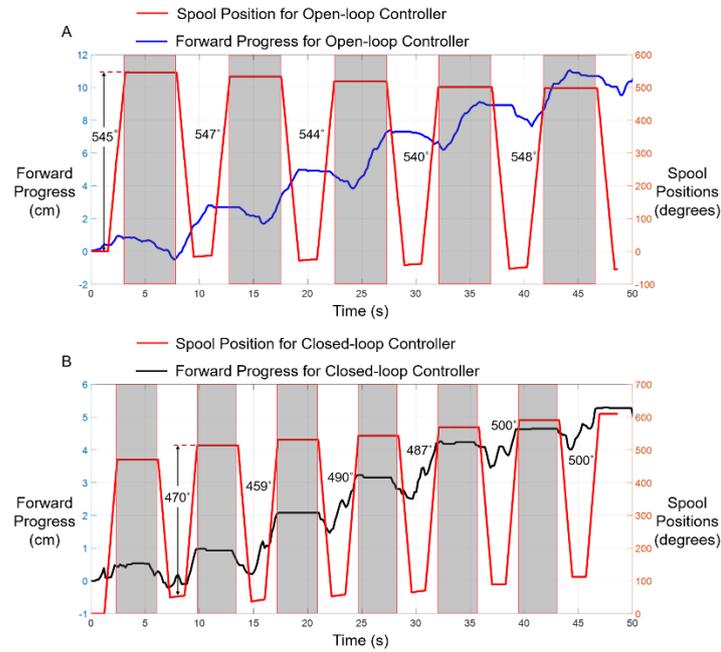
**Fig. 6.** Comparison between (A) open-loop and (B) closed-loop controller. On the left Y-axis is the forward progress, measured using video tracking software, of the second segment during peristaltic locomotion (Note the scale difference in both figures (A) and (B)). Right Y-axis indicates the spool position of the actuator of that segment. Gray boxes are aligned with the spool position indicating anchoring phase. The angle by which the actuators rotate from contraction phase to expansion phase is indicated beside the gray boxes. Overall, in a span of 50 seconds, the total forward progress achieved by the open-loop controller is 10.43cm in 5 complete waves. In contrast, for the closed loop-controller, forward progress is 5.04cm by the end of the anchor phase of the 7th peristaltic wave.

This soft robot shows the ability to alter its gait pattern in accordance to its environment using a closed-loop controller. With open loop control, the motors continue to rotate even after coming in contact with an external constraint. The actuators rotate for approximately 545˚ in the open-loop controller. For the closed-loop controller, on encountering an external constraint, the actuators stop rotating, thereby causing no further expansion. During this time, the actuators rotate between 459˚ - 500˚. The reduction in degrees rotated causes the peristaltic cycle to move faster, by shortening the time duration of each cycle. The adaptability of the closed-loop controller to its external environment leads to coordinated motion that wastes less energy.

# 6 Conclusions

In this article we discover that in a constrained environment (a) the forward progress under open-loop control is largely due to slip, (b) the actuators work harder and longer in open loop, wasting energy and risking damage to the structure and actuation cables, and (c) the movements of the closed loop robot incur less slip which is a key cause of imprecision during locomotion. However, the robot's overall speed is slowed relative to open loop control, in part due to the reduction in forward slip. With sensors, DiSCo-Worm is capable of reducing slip in both the forward and backward direction.

The FSR data will help to improve the closed loop control for soft robots in future work. From Figure 5A, blue line, the contact forces decrease after initial contact. Whether this is due to structural interdependence of segments or multi-time scale dynamics, this work demonstrates that an anchoring-state force controller will be necessary to prevent early cut-off of soft expansion. Conversely, without such a controller, designing the segment structure for compliance might be a higher priority than developing sensors. On the other hand, in our simulated worm-like robot, the gains in performance were very small unless the phasing of the segments was permitted to adapt [21].

From Figure 6, it can be observed that, for the open loop controller, most of the forward progress for the 2nd segment occurred during the anchoring phase of the wave (58% of the total 10.43 cm). Thus, instead of the segment lifting and progressing forward, the segment drags along the upper and lower surface of the external constraints. For the closed-loop controller, minimal slip was observed during the anchoring phase of peristaltic locomotion ($\sim$0). However, the segment did experience a large amount of backward slip during its contraction phase. An improved controller could solve this problem. In Figure 6, a drift in actuator positions is observed in the closed-loop controller due to inaccuracies in stretch sensors during contraction. We can reduce these sensor inaccuracies using signal processing techniques. Furthermore, it may be valuable to be able to sense shear force in order to detect slip [23].

This work suggests the type of sensors that are valuable for reducing positional uncertainty in worm like motion. Sensory feedback can also protect the robot from damage. Due to continuous rotation, there have been instances where the excess actuation tangles the cable, causing the cable to break. The closed-loop control prevents this from happening. With the sensory feedback, we can develop control that is more precise and allows the robot to navigate through various constrained environments.

The next step is to develop more complex control algorithms for generating and maintaining friction against the ground with the goal of navigating more challenging constrained surfaces.

## Acknowledgments

12

# References

[1]    G. Rateni, M. Cianchetti, G. Ciuti, A. Menciassi and C. Laschi "Design and development of a soft robotic gripper for manipulation in minimally invasive surgery: a proof of concept". in *Meccanica*, *50*(11), pp. 2855-2863, 2015.

[2]    R. Altendorfer, N. Moore, H. Komsuoglu, M. Buehler, H. B. Brown, D. McMordie, U. Saranli, R. Full and D. E. Koditschek, "Rhex: A biologically inspired hexapod runner" in *Autonomous Robots*, *11*(3), pp.207-213, 2001.

[3]    S. Seok, C. D. Onal, K. J. Cho, R. J. Wood, D. Rus and S. Kim, "Meshworm: a peristaltic soft robot with antagonistic nickel titanium coil actuators" in *IEEE/ASME Transactions on mechatronics*, *18*(5), pp.1485-1497, 2013.

[4]    A. Kandhari, A. D Horchler, G. S. Zucker, K. A. Daltorio, H. J. Chiel and R. D. Quinn "Sensing contact constraints in a worm-like robot by detecting load anomalies" *Living Machines Conf.* LNCS, vol. 9793, pp. 97-106, 2016.

[5]    E. V. Mangan, D. A. Kingsley, R. D. Quinn and H. J. Chiel "Development of a peristaltic endoscope" *Proc. IEEE Int. Conf. Robot. Autom.* 347–52, 2002.

[6]    A. D. Horchler, A. Kandhari, K. A. Daltorio, K.C. Moses, J. C. Ryan, K. A. Stultz, E. N. Kanu, K. B. Andersen, J. Kershaw, R. J. Bachmann, H. J. Chiel and R. D. Quinn "Peristaltic locomotion of a modular mesh-based worm robot: precision, compliance, and friction" in *Soft Robotics* **2**(4) 135–45, 2015.

[7]    R. Vaidyanathan, H. J. Chiel and R. D. Quinn "A hydrostatic robot for marine applications" *Robot. Auton. Syst.* **30** 103–13, 2000.

[8]    A. S. Boxerbaum, A. D. Horchler, K. M. Shaw, H. J. Chiel and R. D. Quinn "Worms, waves and robots" *Proc. IEEE International Conference on Robotics and Automation*, pp. 3537-3538, 2012.

[9]    D. Trivedi, C. D. Rahn, W. M. Kier and I. D. Walker "Soft robotics: Biological inspiration, state of the art, and future research" in *Applied Bionics and Biomechanics*, *5*(3), pp.99-117, 2008.

[10]   P. Dario, P. Ciarletta, A. Menciassi and B. Kim "Modeling and experimental validation of the locomotion of endoscopic robots in the colon" in *The International Journal of Robotics Research*, *23*(4-5), pp.549-556, 2004.

[11]   Y. Huang, A. Kandhari, H. J. Chiel, R. D. Quinn and K. A. Daltorio "Mathematical modeling to improve control of mesh body for peristaltic locomotion" in *Conference on Biomimetic and Biohybrid Systems* (pp. 193-203), 2017.

[12]   H. J. Chiel, P. Crago, J. M. Mansour and K. Hathi "Biomechanics of a muscular hydrostat: a model of lapping by a reptilian tongue" in *Biol. Cybern.* **67**(5) 403–15, 1992.

[13]   J. Gray and H. W. Lissmann "Studies in Animal Locomotion VII. Locomotory Reflexes in the Earthworm" in *J. Exp. Biol.* **15** 506–17, 1938.

[14]   E. N. Kanu, K. A. Daltorio, R. D. Quinn and H. J. Chiel "Correlating kinetics and kinematics of earthworm peristaltic locomotion" *Proc. Int. Conf. Biomim. Biohybrid Syst.* **9222** 92–6, 2015.

[15]   K. Mizutani, T. Shimoi, H. Ogawa, Y. Kitamura and K. Oka "Modulation of motor patterns by sensory feedback during earthworm locomotion" in *Neurosci. Res.* 48(4), 457–462, 2004.

[16]   P. J. Mill "Recent developments in earthworm neurobiology" in *Comp. Biochem. Physiol.* 12, pp. 107–115, 1982.

[17]   M. Ikeuchi, T. Nakamura and D. Matsubara "Development of an in-pipe inspection robot for narrow pipes and elbows using pneumatic artificial muscles" *Proc. IEEE/RSJ International Conference on Intelligent Robots and Systems*, pp. 926-931, 2012.

[18]   B. A. Trimmer, A. E. Takesian, B. M. Sweet, C. B. Rogers, D. C. Hake and D. J. Rogers, "Caterpillar locomotion: a new model for soft-bodied climbing and burrowing robots" *International Symposium on Technology and the Mine Problem*, Vol. 1, pp. 1-10, 2006.

[19]   A. M. Bertetto and M. Ruggiu "In-pipe inch-worm pneumatic flexible robot" *Proc. IEEE/ASME International Conference on Advanced Intelligent Mechatronics*, Vol. 2, pp. 1226-1231, 2001.

[20]   T. Tanaka, K. Harigaya and T. Nakamura "Development of a peristaltic crawling robot for long-distance inspection of sewer pipes" *Proc. IEEE/ASME International Conference on Advanced Intelligent Mechatronics*, pp. 1552-1557, 2014.

[21]   K. A. Daltorio, A. S. Boxerbaum, A. D. Horchler, K. M. Shaw, H. J. Chiel and R. D. Quinn "Efficient worm-like locomotion: slip and control of soft-bodied peristaltic robots" in *Bioinspir. Biomim.* **8**(3) 035003, 2013

[22]   Kandhari, A., Huang, Y., Daltorio, K.A., Chiel, H.J. and Quinn, R.D., 2018. Body stiffness in orthogonal directions oppositely affects worm-like robot turning and straight-line locomotion. *Bioinspiration & biomimetics*, *13*(2), p.026003.

[23]   Umedachi, T., Kano, T., Ishiguro, A. and Trimmer, B.A., 2016. Gait control in a soft robot by sensing interactions with the environment using self-deformation. *Royal Society open science*, *3*(12), p.160766.